Atmos. Chem. Phys., 25, 15683–15700, 2025 https://doi.org/10.5194/acp-25-15683-2025 © Author(s) 2025. This work is distributed under the Creative Commons Attribution 4.0 License.





Missing wintertime methane emissions from New York City related to combustion

Luke D. Schiferl¹, Andrew Hallward-Driemeier^{1,2}, Yuwei Zhao^{1,2}, Ricardo Toledo-Crow³, and Róisín Commane^{1,2}

¹Lamont-Doherty Earth Observatory, Columbia University, Palisades, NY 10964, USA
 ²Department of Earth and Environmental Sciences, Columbia University, New York, NY 10027, USA
 ³Advanced Science Research Center, City University of New York, New York, NY 10031, USA

Correspondence: Luke D. Schiferl (schiferl@ldeo.columbia.edu) and Róisín Commane (r.commane@columbia.edu)

Received: 23 January 2025 – Discussion started: 19 March 2025 Revised: 2 October 2025 – Accepted: 5 October 2025 – Published: 17 November 2025

Abstract. Accurately quantifying methane emissions from cities, and understanding the processes that drive these emissions, is important for reaching climate mitigation goals. Methane emissions from New York City metropolitan area (NYCMA), the most populous urban area of the United States, have consistently been underestimated by emission inventories compared to aircraft and satellite observations. In this study, we used continuous rooftop measurements of methane over six winter-to-spring transitions (January-May 2019-2024) to examine the variability of city-scale methane enhancements (ΔCH_4) and estimate methane emissions from the NYCMA. We found large variability in the 10 d mean observed ΔCH_4 ($\sim 50-250$ ppbv) and monthly afternoon methane emissions rates (10.1–30.4 kg s⁻¹) within and between the years of our study period. A recently released highresolution regional methane emission inventory developed for the NYCMA performed better than other global and national inventories against the rooftop observations but still underestimated methane emissions, especially in winter. The estimates of methane emissions correlated with those of carbon monoxide (CO) emissions, determined from coincident measurements, suggesting a common city-scale incomplete combustion source for both methane and CO. Our analysis of these continuous measurements also implies a consistent diurnal cycle in urban methane emissions from the NYCMA, which reveals a potential bias in traditional afternoon-only approaches in this domain. This work highlights the usefulness of a long term, multi-species approach to constrain urban greenhouse gas emissions and their sources.

1 Introduction

Methane (CH₄) is the second most potent greenhouse gas for climate change, with a global warming potential \sim 80 times greater than carbon dioxide (CO₂) over 20 years (Forster et al., 2021). Atmospheric methane has a lifetime of only \sim 9 years (Prather et al., 2012) and thus provides a better opportunity than CO₂ for near-term mitigation of warming with emissions reductions (Jackson et al., 2020; Ocko et al., 2021; UNEP, 2021). The largest global anthropogenic sources of methane to the atmosphere are livestock production, the oil and gas industry, and landfills and other waste, while natural methane emissions come largely from wetlands (Saunois

et al., 2020). However, the trends, magnitude, and variability of these methane emissions sectors remain uncertain (e.g., Tibrewal et al., 2024; Turner et al., 2019). Recently, methane emissions from oil and gas infrastructure (i.e., rural production facilities, pipeline leaks in cities) have received particular attention as mitigation targets (Alvarez et al., 2018; Ocko et al., 2021), highlighting the importance of accurately quantifying baseline methane emissions in order to track the effectiveness of mitigation efforts.

In cities, anthropogenic methane emission sources are expected to be limited to landfills, wastewater treatment plants, and natural gas distribution (pipelines), with some natural

wetland emissions. Previous studies have identified atmospheric methane emissions that were greater than expected from inventories for cities across the world - e.g., in the United States of America (US): Boston (McKain et al., 2015; Sargent et al., 2021); Indianapolis (Lamb et al., 2016); Washington, D.C. (Ren et al., 2018); Los Angeles (Wunch et al., 2016); and Europe: Utrecht, the Netherlands (Maazallahi et al., 2020); Hamburg, Germany (Forstmaier et al., 2023; Maazallahi et al., 2020); Munich, Germany (Chen et al., 2020); Bucharest, Romania (Fernandez et al., 2022). Numerous studies from cities in the US have identified an unexpected correlation between methane emissions and natural gas consumption (e.g., He et al., 2019; Huang et al., 2019; Sargent et al., 2021). Sargent et al. (2021) found methane emissions from Boston did not follow the distribution of natural gas infrastructure, and there was little decrease in emission rates over 8 years, despite concentrated efforts to mitigate leaks from pipelines. Without improved source attribution and understanding of urban methane emission processes, it is unlikely that cities will meet mitigation targets.

The New York City metropolitan area (NYCMA) is the densest and most populated urban region in the US and contains some of the oldest infrastructure of the country. Previous work to measure atmospheric methane in the NYCMA has used airborne data that have focused on snapshot time periods, particularly good weather days in the fall, winter, and spring. For example, using April and May 2018 aircraft observations, Plant et al. (2019) showed that the NY-CMA was by far the largest urban source of methane across the northeast US and that the city emits 3-5 times more methane than estimated by the US national gridded inventory for 2012 (Maasakkers et al., 2016). Additional airborne measurements in November, February, and March over two winters (2018–2020) found methane emissions from the NY-CMA to be 2.4 times higher than the same national inventory (Pitt et al., 2022). Analysis of flights from September 2017 and March 2018 indicated that the observed methane was more likely to be from natural gas than microbial sources around the NYCMA (Floerchinger et al., 2021).

The most recent US national gridded inventory (EPA GHGI v2023, Maasakkers et al., 2023) reduced the estimated methane emissions relative to the previous version (EPA GHGI v2016, Maasakkers et al., 2016) for the NYCMA, thus worsening the underestimate. EPA GHGI v2023 did not include natural gas post-meter methane emissions (assumed 100% combustion efficiency), but the simultaneously released EPA GHGI v2023 with Express Extension (EE) included a post-meter estimate that accounts for $\sim 12\%$ of total methane emissions in our study domain. A recently released higher-resolution regional inventory specific to the NYCMA indicated much greater methane emissions ($\sim 50\%$ higher, including natural gas post-meter) than EPA GHGI v2023 but still underestimated airborne methane observations (Pitt et al., 2024b).

Satellite-based instruments have the potential to provide daily measurements of methane columns across large, diverse regions. However, these observations are limited to only clear sky afternoons, and current shortwave infrared instruments do not produce high-quality data over water, which presents a challenge for observing methane over coastal urban regions like the NYCMA, particularly surrounding the urban core of Manhattan Island. Still, Plant et al. (2022a) estimated the methane emissions from the NY-CMA using TROPOMI data (methane and carbon monoxide – CO – column enhancement ratios) from 37 d of 2019 and found the mean emission rate to be 3-4 times larger than the EPA GHGI v2016, with a confidence interval spanning nearly twice the mean. The national-scale inversion performed by Nesser et al. (2024) using TROPOMI methane columns from 2019 found methane emissions for the NY-CMA to be similar to the aircraft-constrained estimates from Pitt et al. (2022, 2024b). Continuous, in situ measurements bridge the gap in the observing system between airborne and satellite studies by providing additional temporal coverage through all weather and times of day.

In this study, we aimed to quantify and characterize the variability of city-scale methane enhancements (ΔCH_4) and emissions estimates from the NYCMA using continuous rooftop measurements from winter to spring over 6 years (2019–2024). Using an atmospheric transport model, we isolated the impacts of meteorology and emissions changes on the observed ΔCH_4 and evaluated various global, national, and regional gridded methane emission inventories. We then identified changes to NYCMA methane emissions induced by the COVID-19 shutdown of spring 2020 and compared them with observation-informed estimates of coincident CO. Finally, we determined monthly methane and CO emissions estimates for our study period and domain and investigated the variability of these emissions over various timeframes to gain insight into the previously underestimated urban methane emissions sources.

2 Methods

2.1 In situ observations

In this study, we used in situ observations of atmospheric methane abundance from a rooftop observatory in the dense urban core of the NYCMA and from a remote site located generally upwind of the city, which helped determine the abundance of methane entering the domain (i.e., the background).

2.1.1 Rooftop measurements in the urban core

Ambient methane dry-mole fractions (units: ppbv, partsper-billion by volume) were measured at the City University of New York Advanced Science Research Center (ASRC) Rooftop Observatory in Hamilton Heights, West Harlem, Manhattan (40.81534° N, 73.95033° W), a site located 56 m a.g.l. (above ground level) (93 m a.sl. – above sea level) (Fig. S1 in the Supplement). The CUNY ASRC site has been used extensively in recent years as a site representative of high-density urban air around the New York City metropolitan area. It has been the site of long-term studies (Schiferl et al., 2024), instrument characterization studies (Commane et al., 2023; Khare et al., 2022), COVID-19 activity change studies (Cao et al., 2023; Tzortziou et al., 2022) and was the location of atmospheric chemistry focused intensive studies in 2022 and 2023 (e.g., Hass-Mitchell et al., 2024 for the NYC-Mets project). The site sampled air most strongly interacting with the surface of a large area of Upper Manhattan and the Bronx and observed a mixture of methane from thermogenic and microbial sources including from natural gas infrastructure, wastewater treatment plants, and landfills. Additional details of the ASRC site were described in Commane et al. (2023) and Cao et al. (2023).

Several different instruments were used to measure drymole fractions of methane over the 6 consecutive winters and springs (January–May) of the study period (2019–2024) due to varying availability. The instruments used in this study were (i) Picarro G2401-m for 2019, 2020, and 1 January-16 March 2023 (reporting at 0.5–1 Hz), (ii) Picarro G2401 for 2021, 16 March-31 May 2023, and 2024 (reporting at ~ 0.3 Hz), and (iii) Aerodyne SuperDUAL for 2022 (reporting at 1 Hz). Each instrument was calibrated using gas cylinders that were traceable to standards calibrated by the Central Calibration Laboratory (CCL) at the National Oceanographic and Atmospheric Administration (NOAA) Global Monitoring Laboratory (GML) in Boulder, Colorado, USA. CCL maintains the World Meteorological Organization (WMO) methane scale (WMO CH₄ X2004A). The Aerodyne SuperDUAL set-up at ASRC was described in Commane et al. (2023). Simultaneous measurements of dry-mole fractions of carbon monoxide (CO, calibration scale WMO CO X2014A) made at the ASRC site for 2019–2022 were described by Schiferl et al. (2024). Here we extended that record of CO measured at the ASRC site to include January-May 2023-2024.

We calculated the hourly mean methane dry-mole fraction at the ASRC site for hours with at least 50 % valid sub-hourly observations (e.g., at least 1800 1 Hz measurements), which were rounded to the nearest 1 ppbv. Since we were interested in characterizing the methane variability of the entire NYCMA, rather than nearby sources, we removed the local-scale plume observations from the city-scale analysis. In the 1 Hz data, all examples of highly variable methane plumes (i.e., near field sources) were strongly correlated with highly variable CO ($R^2 > 0.99$). Methane observations were categorized as either city- or local-scale using the variability of the co-located CO observations at the ASRC site: hours with a CO standard deviation below 200 ppbv do not contain large plumes and were classified as city-scale. The threshold of 200 ppb for the CO standard deviation was chosen

from a sensitivity analysis to replicate the results of the two-tower approach detailed in Schiferl et al. (2024). The categorization scheme indicated that many of the largest methane peaks were from local-scale sources near the observation site (Fig. S2), as was the case for CO in Schiferl et al. (2024). As these plumes are not representative of the broader city scale, especially in 2020–2023, they were excluded from the analysis. The observed city-scale methane mole fractions had hourly peaks that were generally below 3000 ppbv and accounted for nearly 80 % of the total observed hours. We also calculated the hourly mean CO at the ASRC site and classified hours of city-scale observed CO as for methane.

2.1.2 Remote measurements to constrain domain inflow

We used hourly methane dry-mole fractions for the entire study period from the Picarro G2301 on the Earth Networks tower in Stockholm, New Jersey (SNJ, 41.14356° N, -74.53872° W; 406 m a.s.l., 53 m a.g.l. intake height) as a paired remote background site (see Fig. S1, Sect. 2.2). The SNJ site was described by Karion et al. (2020), and the Earth Networks measurement system module was described by Welp et al. (2013) and Verhulst et al. (2017). All data were calibrated to the NOAA WMO calibration scale (WMO CH₄ X2004A), and data are archived at the National Institute of Standards and Technology (NIST) (Karion et al., 2025).

2.2 Observed methane enhancement calculation

We defined the observed methane enhancement (ΔCH_4) from the NYCMA for each hourly city-scale observation as in Eq. (1):

observed
$$\Delta CH_4$$
 = observed CH_4 – background CH_4 (1)

where the observed ΔCH_4 (units: ppbv) was the observed methane dry-mole fraction with the background methane removed. The background methane accounts for the atmospheric methane entering the study domain prior to being impacted by fluxes from the NYCMA.

To approximate the potential range in background methane, we estimated the rolling hourly 10d background methane in two ways: (i) the fifth percentile of mole fractions at the urban core (ASRC) site using only the city-scale methane observations and (ii) the mean of the methane observations at the remote (SNJ) site, with both methods using data from the previous and following 5 d. These background estimation methods were applied as in Schiferl et al. (2024). We determined a confidence interval (CI) for each hourly background by calculating a distribution of backgrounds using a resampling bootstrap (n = 1000) with replacement over the methane observations for each rolling 10 d window. The background methane mole fractions were variable but most often peaked in late winter and declined toward June (Fig. S3). We also observed an increasing trend in background methane from year-to-year consistent with the

increase in global atmospheric methane. The 95 % CI for each hourly methane background was generally smaller, especially using the remote site method, than the variability in the background over time, which indicated high relative confidence in that background at a given hour. Differences in the background methane calculated from the two methods (an estimation of the background uncertainty) were up to 50 ppbv but were often much lower ($\sim 5{\text -}10\,\text{ppbv}$). Given the position of the remote site in the prevailing upwind direction relative to the largest emitting regions of the NYCMA (Fig. S1), it is unlikely that the NYCMA was heavily sampled at the remote site, except for days with strong east winds. In this case, using the remote site as a background may lead to an underestimate in the magnitude of the observed ΔCH_4 .

Observed ΔCH_4 was calculated for the ASRC site using the observed methane from that site and the distributions of both the urban core fifth-percentile background and the remote background. From the hourly observed ΔCH_4 , we calculated: (i) the 10 d mean observed ΔCH_4 centered on each day of the study period, which allowed us to assess sub-monthly methane variability while removing variability on synoptic timescales, and (ii) the mean observed ΔCH_4 for each 2h period throughout the day (a diurnal pattern) over various periods to assess sub-daily methane variability. These averaging techniques were previously used by Schiferl et al. (2024) to assess the variability of CO from the NY-CMA, but here we estimated the mean observed ΔCH_4 and corresponding CI by calculating a distribution using a resampling bootstrap (n = 1000) with replacement, where the sampled population included the distribution of backgrounds from both methods and the variability of observed methane within each averaging period. As in Schiferl et al. (2024), we only calculated the mean observed ΔCH_4 over averaging periods with at least 50% valid hours. We also recalculated and extended the record of observed ΔCO from Schiferl et al. (2024) at the ASRC site using the urban core fifth-percentile and remote site mean backgrounds to match the time period of study and method for ΔCH_4 (now through 2024). For CO, the remote background was calculated using observations from the regional-scale Air Quality System (AQS) site operated by the Environmental Protection Agency (EPA) site at Cornwall, Connecticut (Fig. S1) as in Schiferl et al. (2024) since the methane remote site (SNJ) did not measure CO. The calibration of the EPA CO observations and their comparability to the ASRC observations are discussed in Schiferl et al. (2024). To avoid biasing the corresponding distributions of mean observed ΔCH_4 and ΔCO , we only used a given background site type (urban core or remote) in the distribution when both methane and CO data were available.

2.3 Methane emission inventories

We used anthropogenic methane emissions from 6 global, national, and regional inventories: (1) the global Emissions

Database for Global Atmospheric Research (EDGAR) v6.0 for 2018 (Crippa et al., 2021), (2) the global EDGAR v8.0 for 2018 (Crippa et al., 2023, 2024), (3) the national EPA Greenhouse Gas Inventory (GHGI) v2016 for 2012 (Maasakkers et al., 2016), (4) the national EPA GHGI v2023 for 2018 (Maasakkers et al., 2023), (5) the national EPA GHGI v2023 with Express Extension (EE) for 2018 (Maasakkers et al., 2023), and (6) the regional Pitt High-Resolution Inventory for 2019 (Pitt et al., 2024b). We used methane inventory emissions from the year 2018, which was the most commonly available year in our set of inventories, or from the closest year to 2018, when that year was not available. All methane emissions inventories used here were available monthly at $0.1^{\circ} \times 0.1^{\circ}$ spatial resolution, except for the Pitt High-Resolution Inventory, which presented an annual emissions rate at $0.02^{\circ} \times 0.02^{\circ}$ over a regional domain centered on the NYCMA. The Pitt High-Resolution Inventory used here was an ensemble comprised of 16 versions with varying scaling assumptions for the wastewater, stationary combustion, and natural gas distribution and post-meter sectors.

According to these inventories, landfills (24.3%-52.8%), wastewater (11.9%-29.4%), and natural gas distribution (8.6%-26.1%) generally provided the largest annual sources of anthropogenic methane emissions from the NYCMA domain, while stationary combustion made up 5.7%-10.9% of the domain total (Table 1). Spatially, landfill and wastewater emissions appeared as point sources, while natural gas distribution emissions followed population density (Figs. S4 and S5). Inventory emissions were greatest in the center of the NYCMA, in the densest urban infrastructure. The New York City (NYC) subdomain (Fig. S1) emitted $\sim 30\%$ of the NYCMA total methane emissions (Table S1 in the Supplement). Large methane sources also existed away from the urban core as waste was transported for storage at suburban and rural landfill sites.

The total methane emissions and the relative contribution of source sectors varied greatly between the inventories. EPA GHGI v2023 had the smallest total methane emissions for NYCMA (5.7 kg s^{-1}) , while EDGAR v6.0 (8.7 kg s^{-1}) had the largest total (Table 1). While the variability between the inventory totals was substantial (up to 3 kg s^{-1}), this uncertainty was much smaller than the range of potential methane emission rates derived from previous observational studies ($\sim 10 \,\mathrm{kg}\,\mathrm{s}^{-1}$). EDGAR v6.0 had very high wastewater emissions compared to the other inventories, with twice the wastewater emissions from EDGAR v8.0 and fourtimes the wastewater emissions from EPA GHGI v2023. EDGAR v6.0 and v8.0 had larger landfill methane emissions than the other inventories, which were twice the landfill emissions from EPA GHGI v2023 and the Pitt High-Resolution Inventory. EDGAR v8.0 had $\sim 50 \%$ higher stationary combustion methane emissions than the other inventories. EPA GHGI v2023 EE and Pitt High-Resolution Inventory included methane emissions from post-meter nat-

Table 1. Annual methane emissions from various inventories by sector and totals for the New York City Metropolitan Area (NYCMA) study domain. The NYCMA area is 46.7×10^3 km² and shown in Fig. S1. Methane emissions inventories are (left to right): Emissions Database for Global Atmospheric Research (EDGAR) v6.0 for 2018 (Crippa et al., 2021), EDGAR v8.0 for 2018 (Crippa et al., 2023, 2024), EPA Greenhouse Gas Inventory (GHGI) v2016 for 2012 (Maasakkers et al., 2016), EPA GHGI v2023 for 2018 (Maasakkers et al., 2023), GHGI v2023 with Express Extension (EE) for 2018 (Maasakkers et al., 2023), and Pitt High-Resolution Inventory for 2019 (Pitt et al., 2024b). For the Pitt High Resolution Inventory, emissions were the mean of the 16 ensemble versions.

Methane inventory emissions	EDGAR	EDGAR	EPA GHGI	EPA GHGI	EPA GHGI	Pitt High-Res.
$[Gg CH_4 yr^{-1}]$	v6.0	v8.0	v2016	v2023	v2023 EE	Inventory
(percentage of total [%])	2018	2018	2012	2018	2018	2019
Landfill	126.0	123.5	102.7	66.7	67.2	64.6
	(46.0)	(52.8)	(44.4)	(37.2)	(31.0)	(24.3)
Natural gas distribution			39.5	40.1	48.4	69.3
	23.6	23.2	(17.1)	(22.4)	(22.3)	(26.1)
Natural gas transmission	(8.6)	(9.9)	14.5	15.1	16.8	10.2
			(6.3)	(8.4)	(7.7)	(3.8)
Natural gas post-meter					26.1	52.3
					(12.0)	(19.7)
Wastewater	80.6	42.4	40.9	22.1	25.8	35.3
	(29.4)	(18.1)	(17.7)	(12.4)	(11.9)	(13.3)
Stationary combustion	15.7	25.6	15.3	17.3	17.2	15.4
	(5.7)	(10.9)	(6.6)	(9.7)	(7.9)	(5.8)
Other	27.9	19.3	18.5	17.7	15.4	18.4
	(10.2)	(8.3)	(8.0)	(9.9)	(7.1)	(6.9)
Total	273.8	234.1	231.4	179.1	216.9	265.6
Total [kg s ⁻¹]	8.68	7.42	7.34	5.68	6.88	8.42

ural gas, and the total emissions from that sector in both inventories were greater than the total natural gas distribution and transmission in EDGAR v6.0 and EDGAR v8.0, although the post-meter emissions in the Pitt High-Resolution Inventory were twice those in EPA GHGI v2023 EE. Generally, EDGAR v6.0 and EDGAR v8.0 had very small natural gas emissions components and larger relative landfill and wastewater emissions than the other inventories.

The differences in methane emissions between inventories were also evident in the spatial distribution of emissions throughout the domain. In the more densely populated NYC subdomain, EDGAR v8.0 had the smallest total methane emissions (1.4 kg s^{-1}) , while the Pitt High-Resolution Inventory had the largest (3.1 kg s⁻¹) (Table S1). EDGAR v8.0 had more methane emissions from stationary combustion than from the wastewater, landfill, and natural gas sectors in NYC, while the natural gas component total alone from the Pitt High-Resolution Inventory was greater than the total for all sectors in EDGAR v8.0. EPA GHGI v2023 fell between EDGAR v8.0 and EPA GHGI v2016 in NYC total emissions and had more similar proportions by sector, but with lower wastewater and greater landfill emission totals, than the Pitt High-Resolution Inventory (and was missing post-meter natural gas completely). EPA GHGI v2023 EE (with post-meter natural gas) was more similar in totals and sector proportions to the Pitt High-Resolution Inventory but had half the post-meter emissions. The higher spatial resolution of the Pitt High-Resolution Inventory allowed for more precise positioning of emission sources within the NYC dense urban core. The spatial variability between some of the inventories may have been due to the incorrect gridding of point sources in some cases, such as the large point sources in New Jersey placed in adjacent grid boxes between inventories (Figs. S4 and S5).

Monthly methane emissions changes in these inventories were minimal when applied over our January-May study period for the NYCMA. For example, EDGAR v6.0 and EPA GHGI v2023 varied less than 3 % month-to-month compared to the mean annual rate. Monthly variability in EDGAR v6.0 was from stationary combustion emissions (5.7 % of annual total), which dropped by more than 50 % from January to May, while the monthly variability in EPA GHGH v2023 was from manure management (1.3 % of annual total), which increased slightly only in May.

Compared to EDGAR v6.0 (Fig. S4), EDGAR v8.0 (Fig. S5) used updated spatial proxies for power generation, industrial facilities, and population distribution (Crippa et al., 2024). Scaling applied to these updated spatial proxies re-

sulted in lower methane emissions in EDGAR v8.0 throughout the NYCMA and a different spatial distribution associated with population-dependent emissions such as wastewater and natural gas distribution. This change contrasts with the point source emissions from landfills which remained relatively constant between the two EDGAR versions.

EPA GHGI v2023 updated methane emissions totals for more recent years using methodological improvements and additional sources, and it better aligned gridding methods with underlying data sets than EPA GHGI v2016 (Maasakkers et al., 2023). In addition to including methane emissions from post-meter natural gas, EPA GHGI v2023 EE provided annual emissions estimates consistent with US methane emission totals for each year but with the same spatial pattern proxy from EPA GHGI v2023 in 2018. Both EPA GHGI v2023 and EPA GHGI v2023 EE had less methane emissions from the NYCMA than EPA GHGI v2016, which previous studies have shown to be too low for this region (e.g., Plant et al., 2019). Most of this methane reduction came from lower emissions from the landfill and wastewater sectors. For 2012, the only coincident year between the EPA GHGI versions, EPA GHGI v2023 was about 7 % lower than EPA GHGI v2016 for the NYCMA and 27 % lower for the NYC subdomain.

We did not apply any interannual emissions scaling to the inventories for our study period due to the large uncertainty of regional and city-scale variability, especially during the COVID-19 shutdown in 2020. Adding interannual variability to the inventories would have unnecessarily confounded the large differences that already existed between the inventories for the most common emissions year. While Crippa et al. (2020) suggested methods to implement diurnal variability in EDGAR using nationwide sector-specific scale factors, we did not apply a diel correction to the emissions of any inventory. Emissions for all inventories were constant throughout the day. Hourly methane emissions variability associated with stationary combustion was expected to be small. Methane emissions from natural sources (i.e., wetlands) are very limited during the winter and spring in the NYCMA, and we did not consider them here.

We also used monthly-varying CO emissions from EDGAR v8.1 (Crippa et al., 2024) for 2018, which were 15% higher on an annual basis for the NYCMA domain and 67% higher for the NYC subdomain than the EDGAR v6.1 CO emissions (Crippa et al., 2018, 2020) evaluated in Schiferl et al. (2024). EDGAR v8.1 included the same updated spatial proxies as in EDGAR v8.0 for methane (Crippa et al., 2024). We used CO emissions from EDGAR rather than from the EPA National Emissions Inventory (NEI) because at this time only EDGAR had provided both CO and CH₄ emissions, uniting the air quality and greenhouse gas emissions communities, as discussed in Schiferl et al. (2024). Hourly CO emissions variability from transportation combustion were expected to be much greater than that from stationary combustion, although we did not apply any hourly

scaling to the CO emissions, consistent with our approach for methane.

2.4 Simulated methane enhancement calculation

We simulated methane enhancements (Δ CH₄) from the NY-CMA for each hour of the study period as in Eq. (2):

simulated
$$\Delta CH_4$$
 = inventory CH_4 emissions flux \times surface influence footprint (2)

where the simulated ΔCH_4 (units: ppbv) was an inventory methane emissions flux (units: nmol m⁻² s⁻¹) multiplied by the 24 h surface influence footprint (units: ppbv (nmol m⁻² s⁻¹)⁻¹). The footprint is an indication of where and for how long the air interacted with the surface of the NYCMA in the previous 24 h. We calculated simulated ΔCH_4 using each of the 6 methane emissions inventories described in Sect. 2.3. We did not consider any loss of atmospheric methane over this 24 h period due to the long lifetime of methane (\sim 9 years, Prather et al., 2012), so all surface methane emissions intercepted by the footprint reach the observation site.

We calculated the surface influence footprint using the Stochastic Time-Inverted Lagrangian Transport (STILT) model driven by NOAA High-Resolution Rapid Refresh (HRRR) meteorology (3 km horizontal, hourly temporal resolution): together referred to as HRRR-STILT (Benjamin et al., 2016; Fasoli et al., 2018). STILT estimates the impact of surface gas fluxes on the atmospheric mole fraction by moving particles backward in time in three dimensions based on the HRRR winds and random turbulence. Interaction between the surface flux and atmospheric mole fraction (the surface influence) happens when particles are present within the lower half of the mixing layer. The accumulated surface influence of the particles was smoothed onto a regular 2-dimensional grid to form a surface influence footprint for ease of combination with the emissions flux inventories.

For this study, we derived the surface influence footprint at 0.01° horizontal and hourly temporal resolution for an integration period of 24 h before the measurement at the ASRC observation site for each hour of the study period to match the hourly mean observations. Our configuration of HRRR-STILT for the NYCMA domain (Fig. S1) was previously used extensively to investigate CO and is described in more detail in Schiferl et al. (2024). While testing the configuration, Schiferl et al. (2024) found that the model configuration for vertical mixing and choice of meteorological product had little effect on the results at this site. They found that only the choice of the minimum Mixing Layer Height (MLH) produced a quantifiable change (> 1 ppbv) in the simulated CO mixing ratio; a 20 ppbv increase in simulated CO enhancement was observed when reducing the minimum MLH from 250 to 150 m (Fig. S7 in Schiferl et al., 2024). We evaluated four possible parameterization of the MLH in STILT and all configurations simulated methane enhancements that differed by less than 1 ppbv in the afternoon, increasing to a maximum of 5 ppbv at night. We also tested the impact of the STILT minimum MLH (150 m vs. 250 m) and meteorological product (HRRR vs. NAMS, North American Mesoscale Forecast System at 12 km horizontal resolution) on our monthly observation-informed emissions estimates (see Sect. 2.5) for 2023 and 2024 and discuss those sensitivity results in Sect. 3.3.

The surface influence footprint from each hourly HRRR-STILT simulation combined with the inventory methane emission flux produced a single simulated ΔCH_4 , which we matched with the valid hourly observed ΔCH_4 at the ASRC site. Mean simulated ΔCH_4 and a corresponding distribution was calculated from the hourly simulated ΔCH_4 as described above for the mean observed ΔCH_4 (over 10 d and 2 h periods). For the Pitt High-Resolution Inventory, the distribution of simulated ΔCH_4 included the ensemble of 16 inventory versions. We also calculated hourly and mean simulated ΔCO using the same HRRR-STILT footprints and CO emissions from EDGAR v8.1.

2.5 Observation-informed methane emissions

We calculated observation-informed methane emissions estimates from the NYCMA for each month (or various multiweek periods during the COVID-19 shutdown, see Sect. 3.3) of the study period as in Eq. (3):

observation-informed CH₄ emissions flux

= domain total inventory
$$CH_4$$
 emissions flux $\times \frac{\text{observed}\Delta CH_4}{\text{simulated}\Delta CH_4}$ (3)

where the distribution of methane emissions was determined using valid hourly observed ΔCH_4 and simulated ΔCH_4 (using annual emissions from the Pitt High-Resolution Inventory) sampled from afternoon (11:00–16:00 EST) hours only and from all hours (24 h). Afternoon emissions estimates required at least 30 valid observation hours, and 24 h estimates required 144 valid observation hours per multi-week period (minimum 6 observations per hour length) to be calculated. This calculation used the relative bias in the methane inventory compared to the methane observations to adjust the initial emissions inventory, and when applied over multi-week timescales to widely sample the study domain, estimated a city-scale methane emissions flux for the NYCMA. A similar method was used to calculate afternoon methane emissions for Boston, Massachusetts by Sargent et al. (2021). We combined the retained distributions of the previously calculated hourly observed and simulated ΔCH_4 such that the resulting observation-informed methane emissions and corresponding CI (calculated at 50% and 95%) account for the background uncertainty, the variability of the observed methane mole fractions within each period, and the ensemble estimate from the Pitt High-Resolution Inventory.

We also calculated the observation-informed CO emissions and corresponding CIs using hourly observed Δ CO and simulated Δ CO (using emissions from EDGAR v8.1) using the same method as for methane. As with calculating the mean 10 d and 2 h observed and simulated enhancements, we only used a given background site type (urban core or remote) in the distribution when the background site type was valid for both methane and CO.

Aggregating hours over the afternoon hours, when the atmospheric transport and mixing is less uncertain, and over the entire day, to increase observational coverage in time and space, provided more confident estimates compared to shorter or more uncertain time periods (e.g., 2 h periods, overnight). These longer aggregation time periods resulted in much narrower confidence intervals, boosting the confidence in our observation-informed emission rates.

2.6 Carbon monoxide (CO) as a combustion tracer

We used coincident observations of CO from the ASRC site as a tracer for incomplete combustion. CO is emitted as a byproduct of combustion when the efficiency of burning a carbon-based fuel source is not optimized, with higher CO emissions per amount of fuel burned indicating a more inefficient combustion process. In the US, CO emission rates have been declining due to improvements in on-road vehicle efficiency, the largest source of CO emissions nationwide (e.g., Hedelius et al., 2021; Lopez-Coto et al., 2022; Yin et al., 2015). Generally, CO emission sources are not co-located with large urban methane emission sources such as landfills, wastewater treatment, and natural gas distribution as the methane from these sources is not actively being combusted, and methane and CO sources are not linked in emissions inventories (outside of wildfires and wood burning). In a wellcontrolled environment, methane can be efficiently burned, but inefficient combustion can lead to large methane emissions (Plant et al., 2022b). Post-meter methane emissions are thought to be from leaks in the local system and do not have well-documented corresponding CO emissions.

Schiferl et al. (2024) characterized CO emissions from the NYCMA using a shorter period of observations from the ASRC site (ending in 2022). That study found large variability in city-scale observed Δ CO, \sim 60 % of which was driven by atmospheric transport meteorology and \sim 40 % of which was driven by emissions changes. Schiferl et al. (2024) also found a substantial underestimate in simulated Δ CO when evaluating CO inventory emissions from EDGAR v6.1 and that the observed Δ CO and associated CO emissions from the transportation sector were unlikely to account for the observed Δ CO variability and magnitude outside of the COVID-19 shutdown of spring 2020.

In this study, we extended the record of hourly observed CO dry-mole fractions at the ASRC site to match the record of methane observations described above. We excluded hours identified as local-scale observations, removed

urban site and remote backgrounds, and calculated simulated ΔCO and observation-informed CO emissions in the same manner as for methane. We used the EDGAR v8.1 CO inventory emissions combined with the observed-to-simulated ΔCO ratio to estimate the city-scale CO emissions. Since CO emissions in EDGAR v8.1 were greater than in EDGAR v6.1, especially in the urban core, simulated ΔCO driven by EDGAR v8.1 were improved over the EDGAR v6.1 CO emissions evaluated by Schiferl et al. (2024) when compared to the observed ΔCO from the ASRC site.

3 Results and discussion

We first use our rooftop observations from six years of winter-to-spring transitions to quantify the magnitude and variability of the city-scale observed methane enhancements (ΔCH_4) from the New York City metropolitan area (NYCMA) and their correlation with enhancements from incomplete combustion (Δ CO). Then, we use our simulations to evaluate and identify bias in various regional-to-global scale methane emission inventories and remove variability in the observations from atmospheric transport (meteorology). Next, we examine diurnal variability in the observed and simulated ΔCH_4 and quantify the changes in methane emissions that occurred relative to known CO emissions declines during the COVID-19 shutdown of spring 2020. Finally, we present monthly observation-informed methane and CO emission rate estimates for the NYCMA over the study period and discuss potential reasons for their correlation.

3.1 City-scale observed ΔCH₄

The observed ΔCH_4 from the NYCMA varied substantially on sub-monthly timescales throughout the winter and spring across all years of the study (Fig. 1). Mean 10 d observed ΔCH_4 ranged from ~ 50 to ~ 250 ppbv. The winters of 2019, 2020, 2022, and 2023 experienced extended large peaks (> 100 ppbv) in observed ΔCH_4 with general declines toward spring. The large peak in 2021 occurred in late March, at the beginning of the transition to spring, while several moderate peaks (50–100 ppb) were observed in winter 2024. In 2019, 2020, and 2023, there was less variability outside of these extended peaks as compared to 2021, 2022, and 2024, which showed several additional small episodes of more elevated ΔCH_4 (~ 50 ppbv).

Observed Δ CO from the NYCMA also varied substantially throughout the study period (Fig. 1), as previously shown by Schiferl et al. (2024) for 2019–2022. The 10d mean observed Δ CH₄ and observed Δ CO varied together throughout the study period (Fig. 1), except for during the COVID-19 shutdown of 2020 (see Sect. 3.3). There was a strong correlation between the observed enhancements of both species (Fig. 2a, $R^2 = 0.61$), with generally higher ob-

served ΔCH_4 and observed ΔCO during winter (January–February) than in spring (April–May). A large portion of the correlation is likely from the variability of atmospheric transport but could also indicate simultaneous emission sources of both methane and CO.

The uncertainty in the 10 d mean observed ΔCH_4 derived from the different background methane calculation methods was most often ~ 10 –25 ppbv but spanned near 0 to 50 ppbv. This uncertainty varied between time periods. For example, the uncertainty in observed ΔCH_4 was notably small throughout 2019 and 2020, while larger uncertainty occurred during March 2022 and more consistently throughout 2023. When combining the uncertainty in the background with the variability of observed methane mole fractions within each averaging window, the 95 % CI of the 10 d mean consistently spanned 20–50 ppbv, with some CI reaching nearly 100 ppbv. The 95 % CI of the 10 d mean observed Δ CO were usually similar to, or slightly smaller than, those for observed ΔCH_4 . The 95 % CI for both species were also mostly smaller than the variability over time in the 10 d mean, which indicates confidence that we can detect changes in observed ΔCH_4 and ΔCO on the 10 d timescale.

3.2 Evaluation of NYCMA methane inventories

We found much more variability in observed ΔCH₄ for the NYCMA than could be explained by existing emissions inventories. Monthly methane emissions for the NYCMA from EDGAR v8.0 and EPA GHGI v2023, the most recent global and US national inventories, only declined by 0.5 % and 2.7 %, respectively, between their seasonal maximum and minimum. For the smaller sub-domain over NYC, the two inventories declined by a similarly small rate (0.9 % for EDGAR v8.0, 1.2 % for EPA GHGI v2023). The Pitt High-Resolution Inventory had no sub-annual variability. Emissions inventories are designed to be longer term snapshots of average emissions and cannot accurately account for all mechanistic variations in emissions processes.

We compared the 10 d mean observed ΔCH_4 with the corresponding simulated ΔCH_4 to evaluate the magnitude in the inventories and to partition the sources of the observed ΔCH_4 variability between meteorology and emissions changes. All six methane emission inventories we examined consistently underestimated the observed ΔCH_4 from the NYCMA (Figs. 3 and S6), and the degree of performance generally followed the domain-wide totals for each inventory (larger emissions performed better).

The Pitt High-Resolution Inventory (Fig. 4a) performed the best of the inventories evaluated, having the smallest underestimate in simulated ΔCH_4 (slope = 0.60 ± 0.05) for the entire study period (Fig. 4b). The comparison differed seasonally, with most of the missing observed ΔCH_4 occurring during with winter, in contrast with the inventory matching or even overestimating the observed ΔCH_4 in the spring (Fig. 4b). The Pitt High-Resolution Inventory cou-

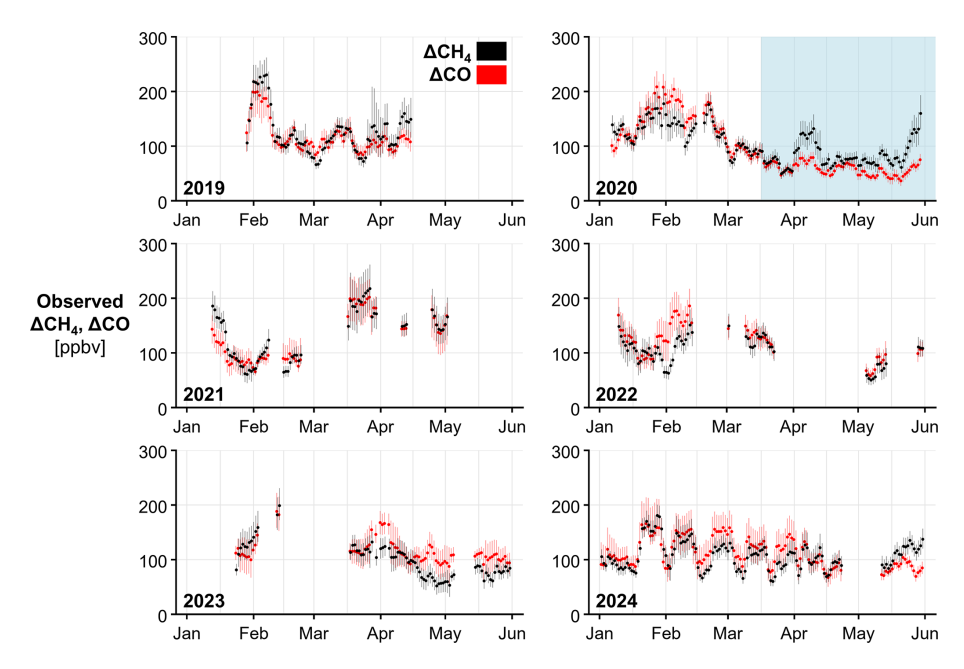


Figure 1. Timeseries of $10 \, d$ mean observed ΔCH_4 (black) and ΔCO (red) for the New York City Metropolitan Area (NYCMA) domain at the urban core ASRC site during January–May 2019–2024. Vertical bars show the 95 % CI (confidence interval) of the mean. Observations are plotted in time at the center of the 10 d averaging period. The COVID-19 shutdown period (15 March–31 May 2020) is shaded in blue.

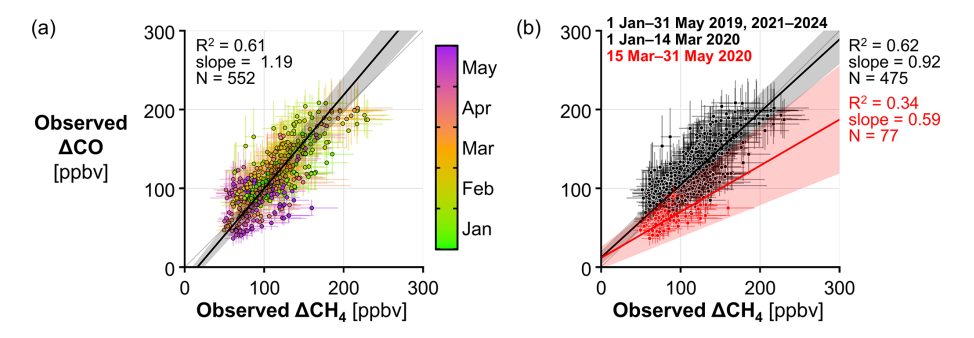


Figure 2. (a) Comparison of 10 d mean observed ΔCH_4 and ΔCO at the urban core ASRC site as in Fig. 1 for the study period colored by day of year. Horizontal (ΔCH_4) and vertical (ΔCO) bars show the 95 % CI of the mean. The linear best fit line, slope, and uncertainty from standard error determined by York fit, the coefficient of determination (R^2), and the number of points considered (N) are shown as indicated. The 1:1 line is shown in dark gray. (b) Comparison of 10 d mean observed ΔCH_4 and ΔCO as in (a) separated and colored by COVID-19 shutdown (15 March-31 May 2020; red) and non-shutdown (all other times; black) periods.

pled with HRRR-STILT also captured peaks and variability in the observed ΔCH_4 not captured by other models (such as in March 2019 and April 2023) (Fig. 3). Simulated ΔCH_4 using EDGAR v6.0 had a slightly greater underestimate (slope = 0.51 \pm 0.04) compared to the observed ΔCH_4 despite a slightly higher domain-wide methane emissions total than the Pitt High-Resolution Inventory. However, the Pitt High-Resolution Inventory emissions for the NYC subdomain were 32 % higher than for EDGAR v6.0 in this region, the area of the domain most heavily sampled by atmospheric observations (Fig. 4a). These discrepancies highlight the importance of accurate and highly resolved spatial emis-

sions distributions for a city with highly variable and heterogeneous sources (Tables 1 and S1).

The EDGAR v6.0 methane inventory performed the best of the global and national inventories compared to the atmospheric observations and the simulated ΔCH_4 were considerably better in magnitude than the more recent inventories such as EDGAR v8.0 (slope = 0.35 \pm 0.03) and EPA GHGI v2023 (slope = 0.29 \pm 0.02). The previous US national inventory, EPA GHGI v2016 (slope = 0.36 \pm 0.03), had a smaller underestimate than the newer version, however, including post-meter emissions in EPA GHGI 2023 EE (slope = 0.39 \pm 0.03) improved the performance of the updated EPA inventory considerably.

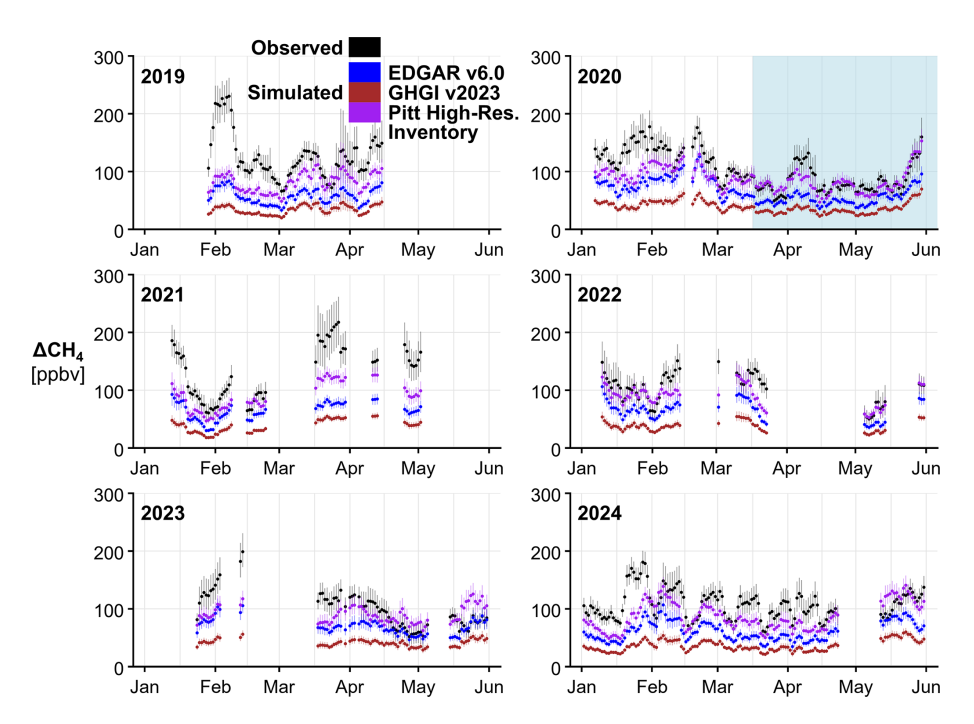


Figure 3. Timeseries of 10 d mean observed Δ CH₄ (black) for the NYCMA domain as in Fig. 1 and simulated Δ CH₄ determined by HRRR-STILT combined with methane emissions from EDGAR v6.0 (blue), EPA GHGI v2023 (brown), and Pitt High-Resolution Inventory (purple). Vertical bars show the 95 % CI of the mean.

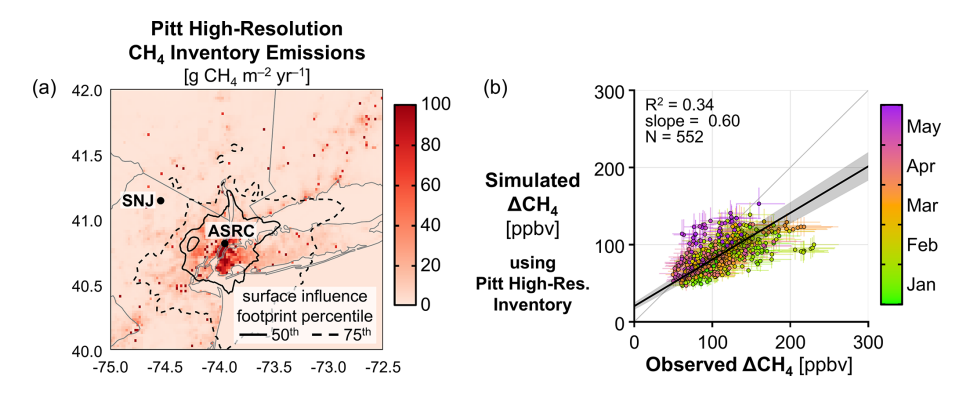


Figure 4. (a) Map of the annual mean methane (CH₄) emissions flux from the Pitt High-Resolution Inventory (Pitt et al., 2024b) for the NYCMA study domain, the locations of the urban core ASRC and remote SNJ observations sites used in the study, and contours of the 50th (solid) and 75th (dashed) percentile mean surface influence footprint from HRRR-STILT used to calculate the mean 10 d simulated Δ CH₄ in (b) for the entire study period. (b) Comparison of 10 d mean observed and simulated Δ CH₄ at the ASRC site as in Fig. 3 colored by day of year, where simulated Δ CH₄ was calculated using the Pitt High-Resolution Inventory. Observed Δ CH₄ are plotted as in Fig. 2. Simulated Δ CH₄ are plotted with horizontal bars for the 95 % CI of the mean. Statistics and annotation are as in Fig. 2.

Our atmospheric observations thoroughly sampled all directions throughout the domain for the study period, according to the surface influence footprints from our transport model simulations, with a slight preference to the southern half of the domain (Fig. 4a). Accounting for the varying atmospheric transport and vertical mixing throughout the study period, which drives nearly all variability in the simulated ΔCH_4 , we found that atmospheric transport and vertical mixing only explained 30 %–43 % of the variability in

observed ΔCH_4 , depending on inventory comparison, based on the calculated R^2 between the observed ΔCH_4 and simulated ΔCH_4 . We note that the Pitt High-Resolution Inventory with no monthly emissions variability was in the middle of this range ($R^2 = 0.34$), indicating that incorporating the monthly emission changes included in the other inventories had limited impact on the outcome. We found that the impact of atmospheric transport and vertical mixing on observed ΔCH_4 in this study was considerably less than was

found by Schiferl et al. (2024) for CO using the same metric and largely same methods, where $\sim 60\,\%$ of the variability in observed ΔCO was due to atmospheric transport and vertical mixing. The weaker correlation for methane than CO implies that the methane emissions may change more across the seasons when calculated on a 10 d time scale. This result is consistent with relatively unchanging seasonal magnitudes of CO emissions from traffic, power generation, and manufacturing, which are sources that are not expected to contribute much to the methane emissions totals in the NYCMA.

3.3 NYCMA methane emissions during the COVID-19 shutdown

We found that the COVID-19 shutdown of spring 2020 had limited impact on the observed ΔCH_4 from the NY-CMA (Fig. 2b). The 10 d mean observed ΔCH_4 centered on 15 March-31 May 2020 were not outside the distribution of observed ΔCH_4 for other study time periods. This result contrasts with the observed ΔCO for the same shutdown period, which decreased by up to 50 ppb below the lower end of the distribution for non-shutdown periods (Fig. 2b). The COVID-19 shutdown was coincident with meteorological conditions favoring lower surface influence (as described by Schifferl et al., 2024), and so the observed enhancements of both species were on the lower end of the observations for the entire study period, but there was no clear step change decrease in observed ΔCH_4 like there was for observed ΔCO .

Using our continuous hourly data record, we also examined the changes in the diurnal pattern of ΔCH_4 prior to and during the COVID-19 shutdown (Fig. 5a). The mean diel cycle of observed ΔCH_4 and simulated ΔCH_4 for the NY-CMA both generally followed the height of the mixing layer: ΔCH_4 peaked in the early morning hours when the layer was lowest, decreased throughout the day as the layer rose, and increased again in the evening. The simulated ΔCH_4 using the Pitt High-Resolution Inventory were generally lower than the observed ΔCH_4 , especially during the daytime hours in winter periods prior to the COVID-19 shutdown, consistent with the mean 10 d underestimate identified above.

Since there was no diurnal variability in the inventory methane emissions, the diurnal variability in the simulated ΔCH_4 was entirely due to changes in the surface influence footprint (i.e., atmospheric transport and vertical mixing) throughout the day. Sensitivity studies of the simulated footprints found that simulated methane could change by up to 1 ppb during the afternoon to 5 ppb overnight depending on the configuration of the model. However, the diel changes in the methane enhancements were of the order 80–200 ppb at night (Fig. 5a) so we estimated the model bias was at most 6 %. The differences in the variability between the observed ΔCH_4 and simulated ΔCH_4 were therefore attributed to changes in the methane emissions which were not included in the inventory. By normalizing the observed ΔCH_4 by the simulated ΔCH_4 , we minimized the impact of meteorology,

thereby isolating only the changes in methane emissions. Using this method, Schiferl et al. (2024) found that most of the CO emissions changes occurred in areas located within 2 h atmospheric transport of the ASRC site and we expect a similar atmospheric transport time for methane. This normalization method produced observation-informed changes in methane emissions for multi-week periods before and during the COVID-19 shutdown (Fig. 5b).

Prior to the COVID-19 shutdown, we found that the normalized ΔCH_4 exhibited a large diurnal cycle with a peak at midday and consistent minimum overnight (Fig. 5b). The daytime peak degraded slightly for the early part of the shutdown (15–31 March), nearly disappeared for early April and returned for the last month (15 April–15 May) of the shutdown. These observed pattern changes imply methane emissions variability that occurred throughout the day and emissions changes that occurred during different time periods of the COVID-19 shutdown. Although not examined closely, these daytime diurnal peaks in normalized ΔCH_4 consistently occurred for all months of the study period.

As part of estimating the observation-informed methane emissions rates when combined with the Pitt High-Resolution Inventory (see Sect. 2.5), we calculated the aggregated 5 h afternoon (11:00–16:00 EST) and 24 h daylong ratios of observed-to-simulated ΔCH_4 . These aggregated normalized ΔCH_4 were similar to the ratios of the coincident 2 h time periods but were produced with much narrower confidence intervals (Fig. 5b). The observed-to-simulated ΔCO ratio for the same time periods showed a larger relative decrease in afternoon when compared to normalized ΔCH_4 (Fig. 5b), consistent with the expected larger decrease in CO emissions (likely from the transportation sector) due to the COVID-19 shutdown.

Afternoon observation-informed methane emission rates from the NYCMA decreased by 22 % (16.2 to $12.6 \,\mathrm{kg}\,\mathrm{s}^{-1}$) between early March and the COVID-19 shutdown of late March 2020 (Table S2). Afternoon CO emission rate reductions were much greater, 49% (44.9 to $22.9 \,\mathrm{kg \, s^{-1}}$) between the same time periods. Clearly, the large reduction in CO emissions was at least partly due to large reductions in the transportation sector due to stay-at-home orders, as expected and observed in other cities (Lopez-Coto et al., 2022; Monteiro et al., 2022). However, Schiferl et al. (2024) also showed that, for the NYCMA, the observed reduction in traffic was not enough to fully explain the reduction in observed Δ CO due to COVID-19 shutdowns. Therefore, it is possible that the methane and CO emissions reductions during the COVID-19 shutdown, from sources other than transportation, were related. It remains uncertain if these COVID-19 shutdown reductions were due to an activity change (e.g., urban population decline, work from home policies) or merely corresponded to seasonal or other non-shutdown emissions mechanisms over the COVID-19 shutdown (e.g., reduction in building heating due to warmer weather).

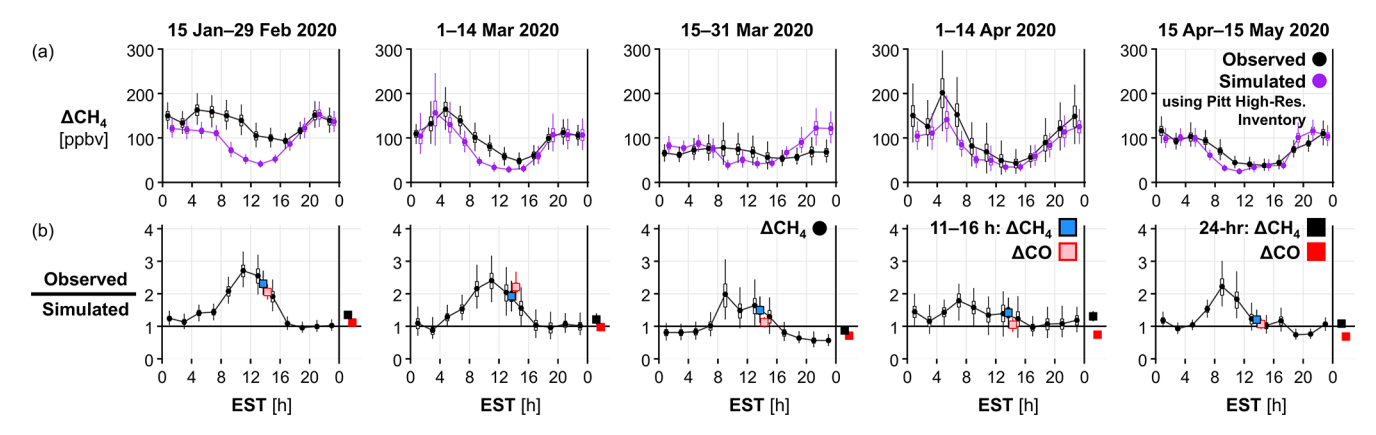


Figure 5. (a) Diurnal timeseries of mean observed ΔCH_4 (black) and simulated ΔCH_4 (purple) using Pitt High-Resolution Inventory for the NYCMA domain at the urban core ASRC site. ΔCH_4 were averaged every 2 h for various periods before and during the peak COVID-19 shutdown (15 January–15 May 2020, left to right). Vertical boxes show the 50 % CI and vertical bars show the 95 % CI of the mean. (b) Diurnal time series (black) of the ratio of observed ΔCH_4 to simulated ΔCH_4 from (a) and the ratio of mean afternoon (11:00–16:00 EST) and mean 24 h observed to simulated ΔCH_4 (blue/black) and ΔCO (red) for each period and plotted in the same matter as in (a). Simulated ΔCO was calculated using CO emissions from EDGAR v8.1.

3.4 Monthly NYCMA observation-informed methane emission rates

Meteorological products (i.e., 3-dimensional wind fields) used to drive the atmospheric transport model are more uncertain at night, for mixing heights especially, and so we focused first on monthly emissions estimates using only afternoon hours. We found the monthly afternoon observationinformed methane emission rates for the NYCMA were highly variable over our study period (Fig. 6a). Generally, the methane emission rates had large, variable peaks in the winter, plateaued during the winter-to-spring transition, and fell to seasonal lows by May. The 95 % CI of these methane emission rate estimates, which included background uncertainties, variability in the observations, and an ensemble of inventory configurations, also varied widely, spanning a range of 4 to $17 \,\mathrm{kg}\,\mathrm{s}^{-1}$. The greatest methane emission rate occurred in January 2021 (30.4 kg s⁻¹), with the lowest methane emission rate in May 2022 ($10.1 \,\mathrm{kg}\,\mathrm{s}^{-1}$; May 2023 and May 2024 are very similar), excluding the COVID-19 shutdown of 2020. Most of the afternoon observation-informed methane emissions rates were much larger than the best-performing emissions inventory, the Pitt High-Resolution Inventory (8.4 kg s^{-1}) . The surface influence footprints used in these afternoon estimates generally sampled the NYCMA domain consistently for all months of the study period (Fig. S7).

The NYCMA observation-informed CO emission rates for the afternoon over the same time periods (Fig. 6b) showed similar trends in variability to those of methane, but without the extreme January peaks. The CO emissions rates for January 2021 and February 2019, for example, were also periods of large methane emission rates. However, several March and April CO emission rates were high, while methane was reduced relative to the cold months. This difference could be due to the relatively large portion of CO emissions from non-heating related sources that are expected to be consistent throughout the winter-to-spring transition (e.g., transportation).

The impact of the COVID-19 shutdown on atmospheric composition was clearly seen in the monthly estimates as well (Fig. 6a and b). A nearly linear month-to-month decrease in emission rates between February and May 2020 resulted in observation-informed CO emissions reductions of 73 %, which was only slightly larger than the relative reduction in methane emissions (67 % over the same period). Afternoon observation-informed emissions rates for the NY-CMA for methane and CO are in Tables S3 and S4, respectively.

The afternoon observation-informed methane and CO emissions rates for the NYCMA were well correlated over our study period (Fig. 6c, $R^2 = 0.59$). Unlike the observed ΔCH_4 : ΔCO dry mole fraction enhancements compared in Sect. 3.1, this relationship between methane and CO emissions accounted for variability in atmospheric transport. We do not know the CH₄: CO emission ratio, nor the modified combustion efficiency of individual incomplete combustion sources (i.e., boilers and other appliances) within our study domain. However, we can expect the CH₄:CO ratio to be variable with each appliance configuration, and so it may change across time and space. We likely observed two competing thermogenic methane source sectors at the rooftop: (1) inefficient consumption of natural gas during peak heating season (January-February), which is correlated with extreme cold events, and (2) intermittent emissions of natural gas during the appliance duty cycle (also known as "slip") (Lindberg et al., 2025). During the winter-to-spring transition, when outdoor temperatures vary around 55 °F, the

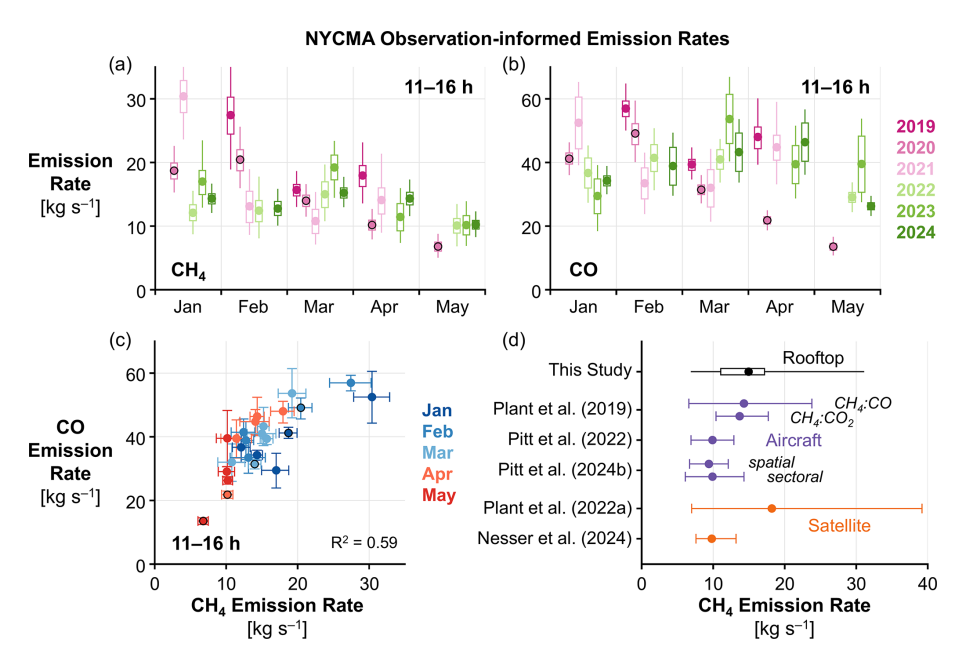


Figure 6. Monthly afternoon (11:00–16:00 EST) observation-informed (a) methane (CH₄) and (b) CO emission rates from the NYCMA for January–May 2019–2024. Vertical boxes show the 50 % CI and vertical bars show the 95 % CI of the emission rate. Monthly emission rates are colored by year according to the legend. Emission rates from 2020 are outlined in black. Individual months without enough data to meet availability threshold to calculate a monthly emission rate are not shown. (c) Comparison of monthly afternoon observation-informed methane and CO emission rates as in (a) and (b). Horizontal (CH₄) and vertical (CO) bars show the 50 % CI of the emission rate. Monthly emission rates are colored by month according to the legend. The R^2 is shown as indicated. (d) Observation-informed methane emission rates from this study (afternoon rooftop observations) compared to methane emission rates for the NYCMA from other studies using aircraft and satellite observations. For this study, the horizontal box shows the 50 % CI and the horizontal bar shows the 95 % CI of the mean emission rate. For other studies, the definition of emission rate point and horizontal bars varies by study-specific method.

threshold below which all buildings are required to be heated by NYC laws (Chapter 2, 2025), boilers will repeatedly cycle. This evidence suggests a common source of methane and CO emissions, which may be related to stationary incomplete combustion. Further study is required to isolate and quantify these processes in more detail.

Our estimates for NYCMA afternoon methane emission rates overlap with methane emissions estimates from previous airborne and satellite studies, which also focused on the afternoon period only (Fig. 6d). Our long-term in situ measurements spanned a greater range of methane emissions, especially at the high end of studies using in situ measurements. Regional inversions using aircraft data by Pitt et al. (2022, 2024b) and a national inversion using satellite data by Nesser et al. (2024) found optimized methane emissions from the NYCMA on the lower end $(9.4-10.5 \text{ kg s}^{-1})$ of our estimates but with narrow uncertainty. Plant et al. (2019) used CH₄: CO and CH₄: CO₂ ratios from aircraft data and inventories to estimate methane emissions for the NYCMA and found similar mean emissions estimates using both methods close to our mean estimate, but their estimate using CH₄: CO had a much larger uncertainty range, which is similar to our range that combines uncertainty and variability throughout our study period. Plant et al. (2022a) used satellite column CH₄: CO ratios to estimate methane emissions, the uncertainty of which spanned our entire range of emissions estimates. All these airborne and satellite studies used the US Census Bureau Topologically Integrated Geographic Encoding and Referencing (TIGER) domain for New York–Newark, which contains $\sim 70\,\%$ of the total emissions of Pitt High-Resolution Inventory used in our study. We note that the airborne studies were restricted to weather conditions that are suitable for flight and satellite studies were restricted to clear-sky days when the methane plume did not move out to sea.

We tested the sensitivity of our observation-informed emissions estimates to assumptions in the transport model in two ways: (1) by lowering the minimum MLH from 250 m (default) to 150 m when STILT is driven by HRRR, and (2) by driving STILT with NAMS instead of HRRR. We found a consistent reduction in afternoon emissions estimates when lowering the HRRR minimum MLH, with a mean decrease of 13 % for methane and 10 % for CO emissions over 2023 and 2024 (Fig. S8). Using NAMS meteorology resulted in similar drops in mean methane (13 %) and CO (16 %) emissions estimates, but with a larger range of changes across months (\sim 50 % reduction to \sim 25 % increase in individual months) which weakened the winter-

to-spring emissions relationship compared to the default HRRR-STILT configuration. Given the heterogeneity of the complex NYCMA landscape, the differences in emissions estimates are more likely to be due to the spatial resolution of meteorological product (HRRR: 3 km, NAMS: 12 km) than MLH errors for the afternoon time periods.

The methane and CO emission estimates for this study (Fig. 6) and in previous studies used afternoon observations only, because there is greater confidence in the atmospheric transport processes used to interpret the observations during this tim emission rates using all observations for a given month (24 h rate), we found consistently lower emissions rates for both methane and CO (Fig. S9a and b). The 24h emission rates for methane and CO were similarly correlated ($R^2 = 0.53$) as they were using afternoon hours only and maintained a similar winter-to-spring decline (Fig. S9c). The consistent difference between the afternoon and 24 h emission rates suggests a diurnal cycle in emissions, which is well-known for CO emissions (traffic, human activity), but had not been, to our knowledge, previously inferred for urban methane emissions. These diurnal emissions patterns were not included in methane inventories nor in the CO inventories used here. If related to combustion, the methane and CO emissions from building heating sources could be greater during the day when commercial and industrial buildings increase heating temperature as occupancy increases. The combination of many hours to produce the monthly 24 h emissions estimates resulted in narrower confidence intervals compared to the afternoon-only emission estimates, further supporting the possibility of diurnal cycle for urban methane emissions. The 24 h observation-informed methane emissions estimates were also more consistent with the inventories evaluated here. CO emissions studies (e.g., Lopez-Coto et al., 2022) apply a daytime correction given the assumed diurnal pattern of CO emissions, so a similar correction may be needed for methane as well to avoid biasing observational-constrained methane emissions too high. The surface influence footprints used in the 24 h emission rate estimates were more balanced in all directions and more contained within the NYC subdomain than when using only the afternoon hours (Figs. S7 and S10), and this implies more sensitivity to larger emissions sources in the urban core on average. The 24h observation-informed emissions rates for the NYCMA for methane and CO for each month January-May for 2019-2024 are shown in Tables S5 and S6, respectively. Our sensitivity analysis of the atmospheric transport model for the 24h emissions estimates found that reducing the minimum MLH consistently lowered the estimated emissions for the NYCMA (mean CH₄ by 21 %, mean CO by 19%) (Fig. S8). Using NAMS reduced the mean 24h estimated emissions by similar relative amounts (CH₄ by 15 %, CO by 20%), although the impact of NAMS on emissions ranged from $\sim 30 \,\%$ reduction to $\sim 15 \,\%$ increase depending on the month across both species.

4 Conclusions

Using in-situ rooftop observations, this study found unexpected variability in atmospheric methane mole fractions, city-scale enhancements, and methane emission rates from the New York City Metropolitan Area (NYCMA) over six winter-to-spring transition periods. Our work reveals the power of long-term continuous measurements, since this variability is not captured by favorable weather-only aircraft campaigns or afternoon, clear-sky satellite measurements. Although our analysis to quantify the methane emissions can retain large relative confidence intervals, especially during periods of highly variable observations, an urban core site with precise instrumentation measuring multiple trace gas species can still be very informative, including potentially resolving diurnal methane emissions patterns previously not shown from afternoon-only studies.

Even the best performing methane emissions inventory, developed specifically for the NYCMA at higher resolution, underestimated the observed atmospheric methane during peak emission events in winter. These methane emission peaks were correlated with elevated CO emissions, which provides strong evidence that these unaccounted-for methane emissions are from the same stationary combustion source type as the CO. Clearly, there is a city-scale atmospheric impact of combustion emissions, but we do not know how widespread the source type is or if there are a few large source points or many small ones. Examining the characteristics of the local-scale measurements removed from the analysis here may help answer these questions.

Future studies should also focus on approximating the stationary incomplete combustion sources based on relationships with temperature or other environmental factors and knowledge of urban stationary combustion systems (i.e., building boilers). Given the uncertainties previously discussed, we need additional sites with 24 h year-round atmospheric measurements of methane and CO, collocated meteorological observations, and systematic evaluation of reanalysis and forecast products, especially at night, to improve the continuous quantification of methane and CO emissions and define their source apportionment. Discovering a mechanistic driver for the methane emissions variability related to incomplete combustion will allow for these emissions estimates to be improved and included in future inventories enabling stakeholders to properly target all potential methane emission sources and track and have confidence in the progress of greenhouse gas emission mitigation efforts.

Data availability. Data that support the findings of this study are available as listed below:

– ASRC Rooftop methane (CH₄) observations and NYCMA observed and simulated Δ CH₄, with coincident carbon monoxide (CO) observations and Δ CO [Dataset]: Dryad https://doi.org/10.5061/dryad.ghx3ffc0g (Schiferl et al., 2025);

- Stockholm, New Jersey (SNJ) methane observations: https://doi.org/10.18434/MDS2-3765 (Karion et al., 2025);
- EDGAR v6.0 methane emissions: https://edgar.jrc.ec.europa.eu/dataset_ghg60 (last access: 16 June 2023);
- EDGAR v8.0 methane emissions: https://edgar.jrc.ec.europa. eu/dataset_ghg80 (last access: 8 July 2024);
- EPA GHGI v2016 methane emissions: https://www.epa.gov/ghgemissions/gridded-2012-methane-emissions (US EPA, 2016);
- EPA GHGI v2023 and EPA GHGI v2023 EE methane emissions: https://doi.org/10.5281/zenodo.8367082 (McDuffie et al., 2023);
- Pitt High-Resolution Inventory methane emissions: https://doi.org/10.18434/MDS2-2915 (Pitt et al., 2024a);
- EPA Cornwall CO observations: https://aqs.epa.gov/aqsweb/ airdata/download_files.html (last access: 1 November 2024);
- EDGAR v8.1 CO emissions: https://edgar.jrc.ec.europa.eu/ dataset_ap81 (last access: 8 July 2024);
- STILT model: https://uataq.github.io/stilt/#/ (last access: 8 November 2019);
- HRRR ARL files: https://www.ready.noaa.gov/archives.php (last access: 8 July 2024).

Supplement. The supplement related to this article is available online at https://doi.org/10.5194/acp-25-15683-2025-supplement.

Author contributions. LDS and RC designed the study. RC, AHD, and YZ provided calibrated ASRC methane and CO measurements. RTC supported ASRC measurements. LDS performed STILT simulations and primary analysis of observation-model comparison. RC and YZ assisted the analysis. LDS wrote the paper. All co-authors contributed to the preparation of the manuscript.

Competing interests. The contact author has declared that none of the authors has any competing interests.

Disclaimer. Publisher's note: Copernicus Publications remains neutral with regard to jurisdictional claims made in the text, published maps, institutional affiliations, or any other geographical representation in this paper. While Copernicus Publications makes every effort to include appropriate place names, the final responsibility lies with the authors. Views expressed in the text are those of the authors and do not necessarily reflect the views of the publisher.

Acknowledgements. This work was supported by the New York State Energy Research and Development Authority (NYSERDA; contract no. 183867), by NOAA research grants (NA20OAR4310306; NA21OAR4310235), and by Columbia University Department of Earth and Environmental Sciences. The authors thank John Mak, Lee Murray, Anna Karion, and Cody Floerchinger for instrumentation and measurement support,

the Advanced Science Research Center (ASRC) for hosting the measurements at the ASRC Rooftop Observatory, and Bronte Dalton and Savannah Ferretti for helpful discussions. We also thank the STILT development team and the R Project community for analysis and plotting tools, especially the ggplot2, ggpattern, magick, anytime, lubridate, raster, and cowplot packages.

Financial support. This research has been supported by the New York State Energy Research and Development Authority (contract no. 183867), the National Oceanic and Atmospheric Administration (grant nos. NA20OAR4310306 and NA21OAR4310235), and Columbia University.

Review statement. This paper was edited by Thomas Karl and reviewed by two anonymous referees.

References

Alvarez, R. A., Zavala-Araiza, D., Lyon, D. R., Allen, D. T.,
Barkley, Z. R., Brandt, A. R., Davis, K. J., Herndon, S.
C., Jacob, D. J., Karion, A., Kort, E. A., Lamb, B. K.,
Lauvaux, T., Maasakkers, J. D., Marchese, A. J., Omara,
M., Pacala, S. W., Peischl, J., Robinson, A. L., Shepson,
P. B., Sweeney, C., Townsend-Small, A., Wofsy, S. C., and
Hamburg, S. P.: Assessment of methane emissions from
the U.S. oil and gas supply chain, Science, 361, 186–188,
https://doi.org/10.1126/science.aar7204, 2018.

Benjamin, S. G., Weygandt, S. S., Brown, J. M., Hu, M., Alexander, C. R., Smirnova, T. G., Olson, J. B., James, E. P., Dowell, D. C., Grell, G. A., Lin, H., Peckham, S. E., Smith, T. L., Moninger, W. R., Kenyon, J. S., and Manikin, G. S.: A North American Hourly Assimilation and Model Forecast Cycle: The Rapid Refresh, Mon. Weather Rev., 144, 1669–1694, https://doi.org/10.1175/MWR-D-15-0242.1, 2016.

- Cao, C., Gentner, D. R., Commane, R., Toledo-Crow, R., Schiferl, L. D., and Mak, J. E.: Policy-Related Gains in Urban Air Quality May Be Offset by Increased Emissions in a Warming Climate, Environ. Sci. Technol., 57, 9683–9692, https://doi.org/10.1021/acs.est.2c05904, 2023.
- Chapter 2: Housing Maintenance Code, https://codelibrary.amlegal.com/codes/newyorkcity/latest/NYCadmin/0-0-0-60027 (last access: 9 January 2025), 2025.
- Chen, J., Dietrich, F., Maazallahi, H., Forstmaier, A., Winkler, D., Hofmann, M. E. G., Denier van der Gon, H., and Röckmann, T.: Methane emissions from the Munich Oktoberfest, Atmos. Chem. Phys., 20, 3683–3696, https://doi.org/10.5194/acp-20-3683-2020, 2020.
- Commane, R., Hallward-Driemeier, A., and Murray, L. T.: Intercomparison of commercial analyzers for atmospheric ethane and methane observations, Atmos. Meas. Tech., 16, 1431–1441, https://doi.org/10.5194/amt-16-1431-2023, 2023.
- Crippa, M., Guizzardi, D., Muntean, M., Schaaf, E., Dentener,
 F., van Aardenne, J. A., Monni, S., Doering, U., Olivier,
 J. G. J., Pagliari, V., and Janssens-Maenhout, G.: Gridded emissions of air pollutants for the period 1970—2012

- within EDGAR v4.3.2, Earth Syst. Sci. Data, 10, 1987–2013, https://doi.org/10.5194/essd-10-1987-2018, 2018.
- Crippa, M., Solazzo, E., Huang, G., Guizzardi, D., Koffi, E., Muntean, M., Schieberle, C., Friedrich, R., and Janssens-Maenhout, G.: High resolution temporal profiles in the Emissions Database for Global Atmospheric Research, Sci. Data, 7, 121, https://doi.org/10.1038/s41597-020-0462-2, 2020.
- Crippa, M., Guizzardi, D., Solazzo, E., Muntean, M., Schaaf, E., Monforti-Ferrario, F., Banja, M., Olivier, J. G. J., Grassi, G., Rossi, S., and Vignati, E.: GHG emissions of all world: 2021 report, Publications Office of the European Union, https://publications.jrc.ec.europa.eu/repository/handle/JRC126363 (last access: 20 December 2024), https://doi.org/10.2760/173513, 2021.
- Crippa, M., Guizzardi, D., Schaaf, E., Monforti-Ferrario, F., Quadrelli, R., Risquez Martin, A., Rossi, S., Vignati, E., Muntean, M., Brandao De Melo, J., Oom, D., Pagani, F., Banja, M., Taghavi-Moharamli, P., Köykkä, J., Grassi, G., Branco, A., and San-Miguel, J.: GHG emissions of all world countries: 2023, Publications Office of the European Union, https://publications.jrc.ec.europa.eu/repository/handle/JRC134504 (last access: 20 December 2024), https://doi.org/10.2760/953322, 2023.
- Crippa, M., Guizzardi, D., Pagani, F., Schiavina, M., Melchiorri, M., Pisoni, E., Graziosi, F., Muntean, M., Maes, J., Dijkstra, L., Van Damme, M., Clarisse, L., and Coheur, P.: Insights into the spatial distribution of global, national, and subnational greenhouse gas emissions in the Emissions Database for Global Atmospheric Research (EDGAR v8.0), Earth Syst. Sci. Data, 16, 2811–2830, https://doi.org/10.5194/essd-16-2811-2024, 2024.
- Fasoli, B., Lin, J. C., Bowling, D. R., Mitchell, L., and Mendoza, D.: Simulating atmospheric tracer concentrations for spatially distributed receptors: updates to the Stochastic Time-Inverted Lagrangian Transport model's R interface (STILT-R version 2), Geosci. Model Dev., 11, 2813002824, https://doi.org/10.5194/gmd-11-2813-2018, 2018.
- Fernandez, J. M., Maazallahi, H., France, J. L., Menoud, M., Corbu, M., Ardelean, M., Calcan, A., Townsend-Small, A., van der Veen, C., Fisher, R. E., Lowry, D., Nisbet, E. G., and Röckmann, T.: Street-level methane emissions of Bucharest, Romania and the dominance of urban wastewater, Atmos. Environ. X, 13, 100153, https://doi.org/10.1016/j.aeaoa.2022.100153, 2022.
- Floerchinger, C., Shepson, P. B., Hajny, K., Daube, B. C., Stirm, B. H., Sweeney, C., and Wofsy, S. C.: Relative flux measurements of biogenic and natural gas-derived methane for seven U.S. cities, Elementa, 9, 000119, https://doi.org/10.1525/elementa.2021.000119, 2021.
- Forster, P., Storelvmo, T., Armour, K., Collins, W., Dufresne, J.-L., Frame, D., Lunt, D. J., Mauritsen, T., Palmer, M. D., Watanabe, M., Wild, M., and Zhang, H.: The Earth's Energy Budget, Climate Feedbacks, and Climate Sensitivity, in: Climate Change 2021: The Physical Science Basis, Working Group I Contribution to the Sixth Assessment Report of the Intergovernmental Panel on Climate Change, edited by: Masson-Delmotte, V., Zhai, P., Pirani, A., Connors, S. L., Péan, C., Berger, S., Caud, N., Chen, Y., Goldfarb, L., Gomis, M. I., Huang, M., Leitzell, K., Lonnoy, E., Matthews, J. B. R., Maycock, T. K., Waterfield, T., Yelekçi, O., Yu, R., and Zhou, B., Cambridge University Press, Cambridge, UK and New York, NY, USA, 923–1054, https://doi.org/10.1017/9781009157896.009, 2021.

- Forstmaier, A., Chen, J., Dietrich, F., Bettinelli, J., Maazallahi, H., Schneider, C., Winkler, D., Zhao, X., Jones, T., van der Veen, C., Wildmann, N., Makowski, M., Uzun, A., Klappenbach, F., Denier van der Gon, H., Schwietzke, S., and Röckmann, T.: Quantification of methane emissions in Hamburg using a network of FTIR spectrometers and an inverse modeling approach, Atmos. Chem. Phys., 23, 6897–6922, https://doi.org/10.5194/acp-23-6897-2023, 2023.
- Hass-Mitchell, T., Joo, T., Rogers, M., Nault, B. A., Soong, C.,
 Tran, M., Seo, M., Machesky, J. E., Canagaratna, M., Roscioli,
 J., Claflin, M. S., Lerner, B. M., Blomdahl, D. C., Misztal, P. K.,
 Ng, N. L., Dillner, A. M., Bahreini, R., Russell, A., Krechmer, J.
 E., Lambe, A., and Gentner, D. R.: Increasing Contributions of
 Temperature-Dependent Oxygenated Organic Aerosol to Summertime Particulate Matter in New York City, ACS EST Air, 1,
 113–128, https://doi.org/10.1021/acsestair.3c00037, 2024.
- He, L., Zeng, Z.-C., Pongetti, T. J., Wong, C., Liang, J., Gurney, K. R., Newman, S., Yadav, V., Verhulst, K., Miller, C. E., Duren, R., Frankenberg, C., Wennberg, P. O., Shia, R.-L., Yung, Y. L., and Sander, S. P.: Atmospheric Methane Emissions Correlate With Natural Gas Consumption From Residential and Commercial Sectors in Los Angeles, Geophys. Res. Lett., 46, 8563–8571, https://doi.org/10.1029/2019GL083400, 2019.
- Hedelius, J. K., Toon, G. C., Buchholz, R. R., Iraci, L. T., Podolske, J. R., Roehl, C. M., Wennberg, P. O., Worden, H. M., and Wunch, D.: Regional and Urban Column CO Trends and Anomalies as Observed by MOPITT Over 16 Years, J. Geophys. Res.-Atmos., 126, e2020JD033967, https://doi.org/10.1029/2020JD033967, 2021.
- Huang, Y., Kort, E. A., Gourdji, S., Karion, A., Mueller, K., and Ware, J.: Seasonally Resolved Excess Urban Methane Emissions from the Baltimore/Washington, DC Metropolitan Region, Environ. Sci. Technol., 53, 11285–11293, https://doi.org/10.1021/acs.est.9b02782, 2019.
- Jackson, R. B., Saunois, M., Bousquet, P., Canadell, J. G., Poulter, B., Stavert, A. R., Bergamaschi, P., Niwa, Y., Segers, A., and Tsuruta, A.: Increasing anthropogenic methane emissions arise equally from agricultural and fossil fuel sources, Environ. Res. Lett., 15, 071002, https://doi.org/10.1088/1748-9326/ab9ed2, 2020.
- Karion, A., Callahan, W., Stock, M., Prinzivalli, S., Verhulst, K. R., Kim, J., Salameh, P. K., Lopez-Coto, I., and Whetstone, J.: Greenhouse gas observations from the Northeast Corridor tower network, Earth Syst. Sci. Data, 12, 699–717, https://doi.org/10.5194/essd-12-699-2020, 2020.
- Karion, A., DiGangi, E., Prinzivalli, S., Draper, C., Baldelli, S., Fain, C., Biggs, B., Stock, M., Michalak, B., Salameh, P., Jooil, K., Lueker, T., and Whetstone, J.: Observations of carbon dioxide (CO₂), methane (CH₄), and carbon monoxide (CO) mole fractions from the NIST Northeast Corridor urban testbed (1.3.0), NIST [data set], https://doi.org/10.18434/MDS2-3765, 2025.
- Khare, P., Krechmer, J. E., Machesky, J. E., Hass-Mitchell, T., Cao,
 C., Wang, J., Majluf, F., Lopez-Hilfiker, F., Malek, S., Wang,
 W., Seltzer, K., Pye, H. O. T., Commane, R., McDonald, B.
 C., Toledo-Crow, R., Mak, J. E., and Gentner, D. R.: Ammonium adduct chemical ionization to investigate anthropogenic oxygenated gas-phase organic compounds in urban air, Atmos.

- Chem. Phys., 22, 14377–14399, https://doi.org/10.5194/acp-22-14377-2022, 2022.
- Lamb, B. K., Cambaliza, M. O. L., Davis, K. J., Edburg, S. L., Ferrara, T. W., Floerchinger, C., Heimburger, A. M. F., Herndon, S., Lauvaux, T., Lavoie, T., Lyon, D. R., Miles, N., Prasad, K. R., Richardson, S., Roscioli, J. R., Salmon, O. E., Shepson, P. B., Stirm, B. H., and Whetstone, J.: Direct and Indirect Measurements and Modeling of Methane Emissions in Indianapolis, Indiana, Environ. Sci. Technol., 50, 8910–8917, https://doi.org/10.1021/acs.est.6b01198, 2016.
- Lindberg, J., Trojanowski, R., Galvin, S., and Butcher, T.: Climate and health-relevant pollutant emissions from oil and natural gas boilers, J. Air Waste Manage. Assoc., 75, 789–807, https://doi.org/10.1080/10962247.2025.2547634, 2025.
- Lopez-Coto, I., Ren, X., Karion, A., McKain, K., Sweeney, C., Dickerson, R. R., McDonald, B. C., Ahn, D. Y., Salawitch, R. J., He, H., Shepson, P. B., and Whetstone, J. R.: Carbon Monoxide Emissions from the Washington, DC, and Baltimore Metropolitan Area: Recent Trend and COVID-19 Anomaly, Environ. Sci. Technol., 56, 2172–2180, https://doi.org/10.1021/acs.est.1c06288, 2022.
- Maasakkers, J. D., Jacob, D. J., Sulprizio, M. P., Turner, A. J., Weitz, M., Wirth, T., Hight, C., DeFigueiredo, M., Desai, M., Schmeltz, R., Hockstad, L., Bloom, A. A., Bowman, K. W., Jeong, S., and Fischer, M. L.: Gridded National Inventory of U.S. Methane Emissions, Environ. Sci. Technol., 50, 13123– 13133, https://doi.org/10.1021/acs.est.6b02878, 2016.
- Maasakkers, J. D., McDuffie, E. E., Sulprizio, M. P., Chen, C., Schultz, M., Brunelle, L., Thrush, R., Steller, J., Sherry, C., Jacob, D. J., Jeong, S., Irving, B., and Weitz, M.: A Gridded Inventory of Annual 2012–2018 U.S. Anthropogenic Methane Emissions, Environ. Sci. Technol., 57, 16276–16288, https://doi.org/10.1021/acs.est.3c05138, 2023.
- Maazallahi, H., Fernandez, J. M., Menoud, M., Zavala-Araiza, D., Weller, Z. D., Schwietzke, S., von Fischer, J. C., Denier van der Gon, H., and Röckmann, T.: Methane mapping, emission quantification, and attribution in two European cities: Utrecht (NL) and Hamburg (DE), Atmos. Chem. Phys., 20, 14717–14740, https://doi.org/10.5194/acp-20-14717-2020, 2020.
- McDuffie, E., E., Maasakkers, J., D., Sulprizio, M., P., Chen, C., Schultz, M., Brunelle, L., Thrush, R., Steller, J., Sherry, C., Jacob, D., J., Jeong, S., Irving, B., and Weitz, M.: Gridded EPA U.S. Anthropogenic Methane Greenhouse Gas Inventory (gridded GHGI) (v1.0), Zenodo [data set], https://doi.org/10.5281/zenodo.8367082, 2023.
- McKain, K., Down, A., Raciti, S. M., Budney, J., Hutyra, L. R., Floerchinger, C., Herndon, S. C., Nehrkorn, T., Zahniser, M. S., Jackson, R. B., Phillips, N., and Wofsy, S. C.: Methane emissions from natural gas infrastructure and use in the urban region of Boston, Massachusetts, P. Natl. Acad. Sci. USA, 112, 1941–1946, https://doi.org/10.1073/pnas.1416261112, 2015.
- Monteiro, V., Miles, N. L., Richardson, S. J., Turnbull, J., Karion, A., Kim, J., Mitchell, L., Lin, J. C., Sargent, M., Wofsy, S., Vogel, F., and Davis, K. J.: The impact of the COVID-19 lockdown on greenhouse gases: a multi-city analysis of in situ atmospheric observations, Environ. Res. Commun., 4, 041004, https://doi.org/10.1088/2515-7620/ac66cb, 2022.
- Nesser, H., Jacob, D. J., Maasakkers, J. D., Lorente, A., Chen, Z., Lu, X., Shen, L., Qu, Z., Sulprizio, M. P., Winter, M., Ma, S.,

- Bloom, A. A., Worden, J. R., Stavins, R. N., and Randles, C. A.: High-resolution US methane emissions inferred from an inversion of 2019 TROPOMI satellite data: contributions from individual states, urban areas, and landfills, Atmos. Chem. Phys., 24, 5069–5091, https://doi.org/10.5194/acp-24-5069-2024, 2024.
- Ocko, I. B., Sun, T., Shindell, D., Oppenheimer, M., Hristov, A. N., Pacala, S. W., Mauzerall, D. L., Xu, Y., and Hamburg, S. P.: Acting rapidly to deploy readily available methane mitigation measures by sector can immediately slow global warming, Environ. Res. Lett., 16, 054042, https://doi.org/10.1088/1748-9326/abf9c8, 2021.
- Pitt, J. R., Lopez-Coto, I., Hajny, K. D., Tomlin, J., Kaeser, R., Jayarathne, T., Stirm, B. H., Floerchinger, C. R., Loughner, C. P., Gately, C. K., Hutyra, L. R., Gurney, K. R., Roest, G. S., Liang, J., Gourdji, S., Karion, A., Whetstone, J. R., and Shepson, P. B.: New York City greenhouse gas emissions estimated with inverse modeling of aircraft measurements, Elementa, 10, 00082, https://doi.org/10.1525/elementa.2021.00082, 2022.
- Pitt, J. R., Lopez Coto, I., Karion, A., Hajny, K. D., Gately, C. K., Hutyra, L. R., Gurney, K. R., Roest, G. S., Liang, J., Gourdji, S., Mueller, K. L., Whetstone, J. R., and Shepson, P. B.: A high-resolution sectoral inventory for use in inverse modelling of New York City methane emissions (1.0.0), NIST [data set], https://doi.org/10.18434/MDS2-2915, 2024a.
- Pitt, J. R., Lopez-Coto, I., Karion, A., Hajny, K. D., Tomlin, J., Kaeser, R., Jayarathne, T., Stirm, B. H., Floerchinger, C. R., Loughner, C. P., Commane, R., Gately, C. K., Hutyra, L. R., Gurney, K. R., Roest, G. S., Liang, J., Gourdji, S., Mueller, K. L., Whetstone, J. R., and Shepson, P. B.: Underestimation of Thermogenic Methane Emissions in New York City, Environ. Sci. Technol., 58, 9147–9157, https://doi.org/10.1021/acs.est.3c10307, 2024b.
- Plant, G., Kort, E. A., Floerchinger, C., Gvakharia, A., Vimont, I., and Sweeney, C.: Large Fugitive Methane Emissions From Urban Centers Along the U.S. East Coast, Geophys. Res. Lett., 46, 8500–8507, https://doi.org/10.1029/2019GL082635, 2019.
- Plant, G., Kort, E. A., Murray, L. T., Maasakkers, J. D., and Aben, I.: Evaluating urban methane emissions from space using TROPOMI methane and carbon monoxide observations, Remote Sens. Environ., 268, 112756, https://doi.org/10.1016/j.rse.2021.112756, 2022a.
- Plant, G., Kort, E. A., Brandt, A. R., Chen, Y., Fordice, G., Gorchov Negron, A. M., Schwietzke, S., Smith, M., and Zavala-Araiza, D.: Inefficient and unlit natural gas flares both emit large quantities of methane, Science, 377, 1566–1571, https://doi.org/10.1126/science.abq0385, 2022b.
- Prather, M. J., Holmes, C. D., and Hsu, J.: Reactive greenhouse gas scenarios: Systematic exploration of uncertainties and the role of atmospheric chemistry, Geophys. Res. Lett., 39, https://doi.org/10.1029/2012GL051440, 2012.
- Ren, X., Salmon, O. E., Hansford, J. R., Ahn, D., Hall, D., Benish, S. E., Stratton, P. R., He, H., Sahu, S., Grimes, C., Heimburger, A. M. F., Martin, C. R., Cohen, M. D., Stunder, B., Salawitch, R. J., Ehrman, S. H., Shepson, P. B., and Dickerson, R. R.: Methane Emissions From the Baltimore-Washington Area Based on Airborne Observations: Comparison to Emissions Inventories, J. Geophys. Res.-Atmos., 123, 8869–8882, https://doi.org/10.1029/2018JD028851, 2018.

- Sargent, M. R., Floerchinger, C., McKain, K., Budney, J., Gottlieb, E. W., Hutyra, L. R., Rudek, J., and Wofsy, S. C.: Majority of US urban natural gas emissions unaccounted for in inventories, P. Natl. Acad. Sci. USA, 118, e2105804118, https://doi.org/10.1073/pnas.2105804118, 2021.
- Saunois, M., Stavert, A. R., Poulter, B., Bousquet, P., Canadell, J. G., Jackson, R. B., Raymond, P. A., Dlugokencky, E. J., Houweling, S., Patra, P. K., Ciais, P., Arora, V. K., Bastviken, D., Bergamaschi, P., Blake, D. R., Brailsford, G., Bruhwiler, L., Carlson, K. M., Carrol, M., Castaldi, S., Chandra, N., Crevoisier, C., Crill, P. M., Covey, K., Curry, C. L., Etiope, G., Frankenberg, C., Gedney, N., Hegglin, M. I., Höglund-Isaksson, L., Hugelius, G., Ishizawa, M., Ito, A., Janssens-Maenhout, G., Jensen, K. M., Joos, F., Kleinen, T., Krummel, P. B., Langenfelds, R. L., Laruelle, G. G., Liu, L., Machida, T., Maksyutov, S., McDonald, K. C., McNorton, J., Miller, P. A., Melton, J. R., Morino, I., Müller, J., Murguia-Flores, F., Naik, V., Niwa, Y., Noce, S., O'Doherty, S., Parker, R. J., Peng, C., Peng, S., Peters, G. P., Prigent, C., Prinn, R., Ramonet, M., Regnier, P., Riley, W. J., Rosentreter, J. A., Segers, A., Simpson, I. J., Shi, H., Smith, S. J., Steele, L. P., Thornton, B. F., Tian, H., Tohjima, Y., Tubiello, F. N., Tsuruta, A., Viovy, N., Voulgarakis, A., Weber, T. S., van Weele, M., van der Werf, G. R., Weiss, R. F., Worthy, D., Wunch, D., Yin, Y., Yoshida, Y., Zhang, W., Zhang, Z., Zhao, Y., Zheng, B., Zhu, Q., Zhu, Q., and Zhuang, Q.: The Global Methane Budget 2000-2017, Earth Syst. Sci. Data, 12, 1561-1623, https://doi.org/10.5194/essd-12-1561-2020, 2020.
- Schiferl, L. D., Cao, C., Dalton, B., Hallward-Driemeier, A., Toledo-Crow, R., and Commane, R.: Multi-year observations of variable incomplete combustion in the New York megacity, Atmos. Chem. Phys., 24, 10129–10142, https://doi.org/10.5194/acp-24-10129-2024, 2024.
- Schiferl, L., Commane, R., Hallward-Driemeier, A., Zhao, Y, and Toledo-Crow, R.: ASRC Rooftop methane (CH₄) observations and NYCMA observed and simulated ΔCH4, with coincident carbon monoxide (CO) observations and ΔCO, Dryad [data set], https://doi.org/10.5061/dryad.ghx3ffc0g, 2025.
- Tibrewal, K., Ciais, P., Saunois, M., Martinez, A., Lin, X., Thanwerdas, J., Deng, Z., Chevallier, F., Giron, C., Albergel, C., Tanaka, K., Patra, P., Tsuruta, A., Zheng, B., Belikov, D., Niwa, Y., Janardanan, R., Maksyutov, S., Segers, A., Tzompa-Sosa, Z. A., Bousquet, P., and Sciare, J.: Assessment of methane emissions from oil, gas and coal sectors across inventories and atmospheric inversions, Commun. Earth Environ., 5, 1–12, https://doi.org/10.1038/s43247-023-01190-w, 2024.

- Turner, A. J., Frankenberg, C., and Kort, E. A.: Interpreting contemporary trends in atmospheric methane, P. Natl. Acad. Sci. USA, 116, 2805–2813, https://doi.org/10.1073/pnas.1814297116, 2019.
- Tzortziou, M., Kwong, C. F., Goldberg, D., Schiferl, L., Commane, R., Abuhassan, N., Szykman, J. J., and Valin, L. C.: Declines and peaks in NO₂ pollution during the multiple waves of the COVID-19 pandemic in the New York metropolitan area, Atmos. Chem. Phys., 22, 2399–2417, https://doi.org/10.5194/acp-22-2399-2022, 2022.
- UNEP United Nations Environment Programme and Climate and Clean Air Coalition: Global Methane Assessment: Benefits and Costs of Mitigating Methane Emissions, United Nations Environment Programme, Nairobi, https://www.unep.org/resources/report/global-methane-assessment-benefits-and-costs-mitigating-methane-emissions (last access: 29 December 2024), 2021.
- US EPA: Gridded 2012 Methane Emissions, https://www.epa.gov/ghgemissions/gridded-2012-methane-emissions (last access: 27 December 2024), 2016.
- Verhulst, K. R., Karion, A., Kim, J., Salameh, P. K., Keeling, R. F., Newman, S., Miller, J., Sloop, C., Pongetti, T., Rao, P., Wong, C., Hopkins, F. M., Yadav, V., Weiss, R. F., Duren, R. M., and Miller, C. E.: Carbon dioxide and methane measurements from the Los Angeles Megacity Carbon Project – Part 1: calibration, urban enhancements, and uncertainty estimates, Atmos. Chem. Phys., 17, 8313–8341, https://doi.org/10.5194/acp-17-8313-2017, 2017.
- Welp, L. R., Keeling, R. F., Weiss, R. F., Paplawsky, W., and Heckman, S.: Design and performance of a Nafion dryer for continuous operation at CO₂ and CH₄ air monitoring sites, Atmos. Meas. Tech., 6, 1217–1226, https://doi.org/10.5194/amt-6-1217-2013, 2013.
- Wunch, D., Toon, G. C., Hedelius, J. K., Vizenor, N., Roehl, C. M., Saad, K. M., Blavier, J.-F. L., Blake, D. R., and Wennberg, P. O.: Quantifying the loss of processed natural gas within California's South Coast Air Basin using long-term measurements of ethane and methane, Atmos. Chem. Phys., 16, 14091–14105, https://doi.org/10.5194/acp-16-14091-2016, 2016.
- Yin, Y., Chevallier, F., Ciais, P., Broquet, G., Fortems-Cheiney, A., Pison, I., and Saunois, M.: Decadal trends in global CO emissions as seen by MOPITT, Atmos. Chem. Phys., 15, 13433–13451, https://doi.org/10.5194/acp-15-13433-2015, 2015.